MICROWAVE ABSORPTION PROPERTIES OF ABSORBER BASED ON POLYANILINE COATED POROUS CARBONYL IRON POWDER AND GRAPHENE SHEETS/EPOXY COMPOSITES

Y. Q. YAN[a], H. P. CAI[a*], Z. Q. LIAO[b], H. B. XIAO[c]

[a]*School of Materials Science and Engineering, Wuhan University of Technology, Wuhan 430070, PR China.*

[b]*China Ship Development and Design Center, Wuhan 430064, PR China.*

[c]*Department of Mechanical and Electrical Engineering, Wuhan Technical and Communications, Wuhan 430065, PR China.*

In this paper, a high-efficiency microwave absorbing material has been prepared through a combination of doped polyaniline (PANI)-coated porous-structure carbonyl iron powder (CIP) and a small amount of graphene sheets within bisphenol F epoxy resin. The reflection loss (RL) performance of these composites has been evaluated by electromagnetic attenuation and impedance matching. Compared to compact iron particles, the porous-structure carbonyl iron particles have a higher complex permittivity and permeability that are closely related to their microstructures. The -10 dB absorption bandwidth and the minimum RL of the composite material showed improvement in comparison to the pure graphene sheets composite. The minimum reflection loss reached -45 dB at a thickness of 3.5 mm while the bandwidth with less than -10 dB RL reached up to 4.6 GHz in the range of 10.3 GHz to 15 GHz, with a matching thickness of 2 mm. The improved microwave absorption performance of the hybrid composite is due to the interfacial polarization, enhanced conductivity, and loss of the electromagnetic radiation through increased transmission routes due to multiple reflection.

(Received October 19, 2017; Accepted January 17, 2018)

Keywords: polyaniline, carbonyl iron powder, reflection loss, porous structure , microwave absorbing

1. Introduction

With the rapid development of science and technology, many electronic devices have entered our daily lives and the resultant electromagnetic pollution has become a serious social problem. Therefore, a great deal of attention has been focused on protecting people's health and information security by preventing the leakage of electromagnetic waves [1，2].

Doped conductive polyaniline (PANI) has been extensively studied as a common conductive polymer because of its easy preparation and excellent environmental stability [3]. PANI acts as an electric-loss medium, and can be used for electromagnetic and microwave absorption when combined with magnetic particles [4, 5]. Zhu et al. prepared Fe_3O_4 coated polyaniline hollow sphere nanocomposites, which exhibited excellent absorbing properties and broadband absorption effect, by using an electrostatic self-assembly method [6]. Carbonyl iron powder (CIP) is an inorganic magnetic absorber with excellent magnetic permeability and good heat resistance [7].

*Corresponding authors: 635812383@qq.com

Therefore, the composite obtained by combining CIP with the conductive polymer PANI has excellent prospects as a lightweight broadband absorbing material. However, the most obvious shortcomings of CIP are its high density and easy agglomeration; this necessitates the treatment of CIP to reduce its density, followed by *in situ* polymerization of doped PANI to obtain lightweight broadband absorbing composites [8].

As far as the authors know, no studies have been reported on the electromagnetic wave absorbing properties of composites made up of graphene sheets and doped PANI@ porous CIP. In this work, an excellent absorber was obtained by combining doped PANI@ porous CIP and a small amount of graphene sheets within an epoxy matrix. A notable feature of this work is that *in situ* polymerization of doped PANI on porous CIP was prepared by acidification of the CIP [9]. Further, the doped PANI@ porous CIP composite was synthesized by *in-situ* polymerization. The porous structure of CIP obtained after acidification served two purposes – a reduction in the density and an increase in the specific surface area of the composite. Thus, polyaniline can be polymerized *in-situ* in CIP to form more internal interfaces, which are conducive to the absorption of electromagnetic waves.

2. Experiment

2.1 Synthesis of Doped PANI@ porous CIP

Porous CIP was synthesized using the methods in the literature [10]. For preparation of doped PANI@porous CIP, the porous CIP was placed in an ethanol solution (95 vol.% ethanol& 5 vol.% water) along with 5% (3-aminopropyl)triethoxysilane (APTES). The as prepared solution was stirred vigorously and heated to 60℃. The as-obtained surface-modified porous CIP was placed in deionized water that contained space stabilizers, and the mixture was stirred vigorously for 1 hour. Then the flask was placed in an ice-water bath and the solution was stirred for 1 hour. A mixture of HCl (50 ml, 0.6 M) and aniline (ANI) monomer (ANI to CIP mass ratio of 2: 1) was placed in the flask and then stirred for 1 hour. An ammonium persulfate solution was added to the mixture at a controlled rate as the reaction rate is very fast, and the reaction temperature was controlled at 0-5℃ for 2 hours. Finally, the reaction product was washed at least five times, and subjected to vacuum drying for 12 hours at 50℃.

2.2 Synthesis of Graphene-PANI@ porous CIP/epoxy Composite

The samples have been encoded using abbreviations to facilitate identification, and have been listed in Table 1 along with their corresponding compositions. The mass percentage of graphene sheets is relatively low (~ 5 wt.%). The experimental procedure (containing 40 wt.% PANI@ porous CIP) consisted of a series of steps. First, 1.6 g of PANI@ porous CIP was added to an absolute ethanol solution containing 0.2 g of graphene sheets, followed by sonication for 30 minutes. The solution was dried and then added to 1.63 g of bisphenol F epoxy resin. Modified amine curing agents, weighing 0.57 g and prepared in our laboratory, were added to the mixture followed by stirring for 10 minutes. The mixture was slowly poured into a mold and cured at 60℃ for 4 hours.

2.3 Characterization

The morphology and microstructure of the samples were characterized by X-ray diffraction (XRD, Bruker D8 Advance diffractometer using a Cu Kα source, λ=0.154056 nm) and scanning electron microscopy (SEM, JSM-5610LV), respectively. The electromagnetic parameters of composite materials were obtained by a vector network analyzer, and the reflection loss values were calculated in the 1-18 GHz frequency range by means of reflection/transmission methods [11]. Each composite specimen was processed by a high-resolution engraving machine (se-3230, Woodpecker) to match following size dimensions: 7 mm outside diameter, 3.04 mm inner diameter, and 2 mm thickness. Further, in order to reduce error, the average data of five different samples have been considered.

Table 1: Acronyms and compositions of the samples.

Sample acronym	Composition
20G-PC	20 wt.% PANI@ porous CIP and 5 wt.% Graphene sheets in epoxy
30G-PC	30 wt.% PANI@ porous CIP and 5 wt.% Graphene sheets in epoxy
40G-PC	40 wt.% PANI@ porous CIP and 5 wt.% Graphene sheets in epoxy
5G	5 wt.% Graphene sheets in epoxy

3. Results and discussion

3.1 Structural Characterization

Fig. 1 shows the XRD patterns of graphene sheets, porous CIP, and PANI@ porous CIP. The diffraction peak at 2θ=20-30°(curve (a)), No other diffraction peaks appear [12]. The strong peaks present at ~ 44.5°and 64.9°(Fig. 1*d*) are because of the original CIP and can be indexed to body-centered cubic α-Fe (JCPDS Card No. 06-0696). Other weak characteristic peaks can be attributed to small amounts of impurities, such as α-Fe_2O_3 and Fe_3O_4 [13].

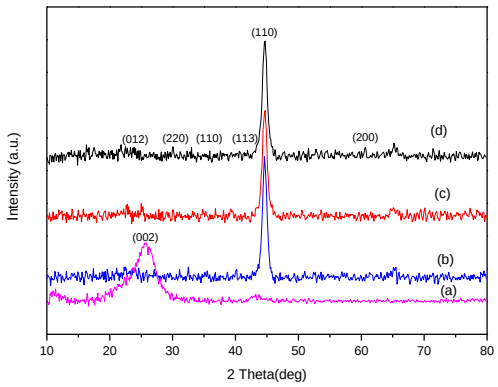

Fig. 1. XRD patterns of (a) GO, (b) PANI@ porous CIP, (c) porous CIP, (d) CIPs.

The microstructure of CIP, porous CIP, and PANI@ porous CIP have been studied with scanning electron microscopy, as shown in Fig. 2. The pure CIP exhibits a smooth spherical surface morphology with an average diameter in the range of 2.5-4.5 μm, as shown in (Fig. 2*a*). After acidification, surface of the carbonyl iron powder becomes rough and forms a porous structure (Fig. 2*b*) that is favorable for the *in-situ* polymerization of ANI on the surface of CIP; this results in a uniform coverage of the entire surface and the pores by PANI (Fig. 2*c*).

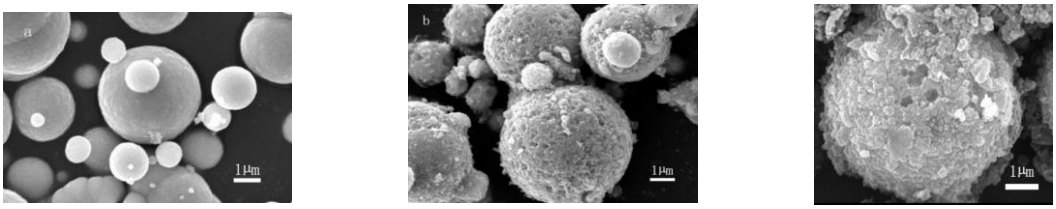

(a) (b) (c)

Fig. 2. SEM images of (a) CIP; (b) porous CIP; (c) PANI@ porous CIP.

3.2 Microwave Absorption Properties

Fig. 3 shows the frequency dependence of the complex permittivity (εr=ε′-jε″) and the complex permeability (μr=μ′-jμ″) for graphene/epoxy and graphene-PANI@ porous CIP/epoxy composites, respectively. The ε′ values of pure graphene/epoxy samples decline from 5.8 to 5.4. In contrast, the ε′ values for 20G-PC remain between 5.8 to 5.5, without any change. The ε′ values for 20G-PC, 30G-PC, and 40G-PC composites increase as the concentration of PANI@porous CIP is increased (Fig. 3*a*). Meanwhile, the ε″ values of the graphene/epoxy samples decline from 1.4 to 1.1. In contrast, the ε″ values for 20G-PC lie in the range of 1.5 to 1.3. The ε″ values for G-PC composites also increase with the increasing concentration of PANI@ porous CIP (Fig. 3*b*). On combining PANI@ porous CIP with a small amount of graphene sheets, the ε′ and ε″ values all showed a marked increase; this may have been caused by an increase in the interface polarization and an electric dipole. [15]. According to the Maxwell–Wagner interfacial polarization principle [16], addition of the filler leads to an increase in the interface and a decrease in the gap between the fillers that will increase the interfacial polarization. Interfacial polarization between any of the interfaces, namely PANI@ porous CIP/epoxy interfaces, graphene/epoxy interfaces, and graphene/PANI@ porous CIP interfaces, is conducive for a significant increase in ε′. Moreover, by increasing the amount of doped PANI@ porous CIP, the effective concentration of graphene can be increased.

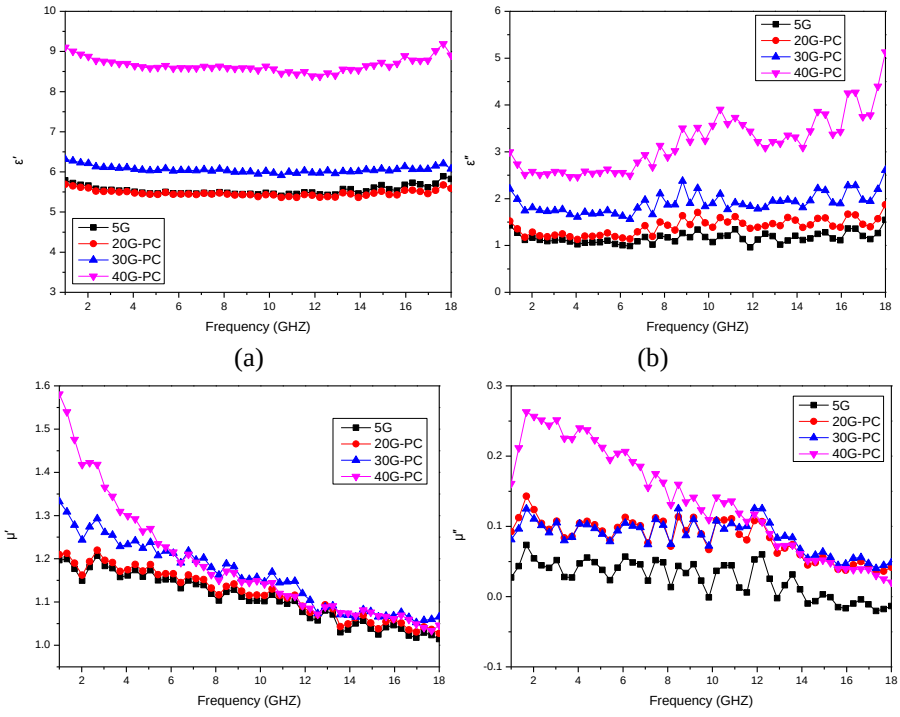

(a) (b)

(c) (d)

Fig. 3. The complex permittivity and complex permeability of the composites

Figs. 3*c* and *d* show the μ′ and μ″ values of the composites. For graphene/epoxy samples, both μ′ and μ″ values are very low because of their weak intrinsic magnetic properties, and the μ′ values showed a significant decline from 1.7 to 1.1 as the frequency was increased. For PANI@ porous CIP and graphene sheets, as the magnetic properties of graphene sheets are weak, the values of μ′ and μ″ remained essentially unchanged. The μ″ values first increase and then decrease for all graphene/PANI@ porous CIP samples, and an apparent impedance peak can be observed at approximately 1.68 GHz. Moreover, the μ″ values rise with an increase in the PANI@ porous CIP loading as it increases the density of the magnetic filler.

In general, the magnetic loss of a material originates mainly from magnetic hysteresis, domain wall resonance, eddy current effect, natural resonance and exchange resonance [17]. The magnetic hysteresis loss is caused mainly by the time lags of the magnetization vector behind external electromagnetic field vector and is negligible in weak applied field. The domain wall resonance occurs only in multidomain materials and usually at lower frequency range (about < 1 GHz) [12]. So neither hysteresis loss nor domain wall resonance is the main contributor to magnetic loss of the absorber. Then if magnetic loss is only from the eddy current effect, $\mu''(\mu')^{-2}f^{-1}$ should be a constant. Fig. 4 shows the dependence of $\mu''(\mu')^{-2}f^{-1}$ values on frequency. The $\mu''(\mu')^{-2}f^{-1}$ first increase and then decrease with the increasing frequency in the 1-11 GHz range and then remain constant in the frequency range of 11-18 GHz, illustrating that the magnetic loss in higher frequency range (11-18 GHz) is caused by eddy current effect. According to Aharoni's theory [18], exchange resonance occurs at a higher resonance frequency than natural resonance. It may be reasonable to deduce that the resonance peak around 1.68 GHz is due to natural resonance, which is attributed to the incorporation of magneto crystalline anisotropy and shape anisotropy of porous CIP magnetic particles.

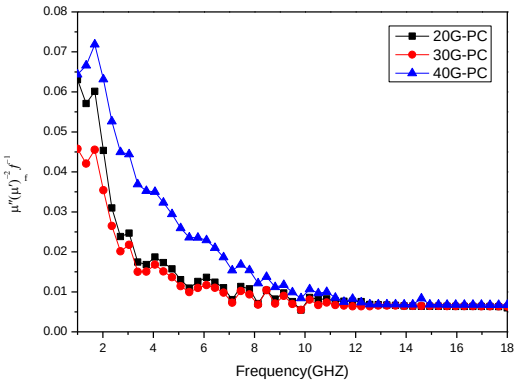

Fig. 4. $\mu''(\mu')^{-2}f^{-1}$ versus frequency curves for Graphene sheets -PANI@ porous CIP/epoxy composite.

The reflection loss (RL) curves of the composites were calculated in the frequency range of 1-18 GHz according to the transmit line theory:

$$RL = 20\log\left|\left(Z_{in}-1\right)/\left(Z_{in}+1\right)\right| \quad (1)$$

$$Z_{in} = \sqrt{\mu_r/\varepsilon_r}\tanh\left(j2\pi fd\sqrt{\mu_r\varepsilon_r}/c\right) \quad (2)$$

Where $\boldsymbol{Z_{in}}$ is the characteristic input impedance of the absorber, $\boldsymbol{f}$ is the frequency of microwaves, $\boldsymbol{d}$ is the thickness of absorber, and $\boldsymbol{c}$ is the velocity of the microwaves in free space. Generally, a material with a reflection loss of less than -10 dB (90% absorption) in the test frequency range

can be considered an effective microwave absorber. In order to better illustrate the microwave absorption properties of composite materials, RL values have been calculated according to the transmission line theory. Fig. 5 shows the RL curves calculated for composites with different thicknesses. The RL of graphene sheets/epoxy composites is relatively low and has no absorption bandwidth below 10 dB, as shown in Fig. 5*a*. On the contrary, Figs. 5*b-d* show that the RL values of graphene sheets-PANI@ porous CIP/epoxy composites are all below -10 dB. For 20G-PC composites, the minimum value of RL (-14.5 dB) is observed for the layer thickness of 3 mm. For 30G-PC composites, the minimum RL is 19.5 dB and the bandwidth less than -10 dB can reach up to 4.0 GHz (from 10.3 to 14.3 GHz). Within the thickness range of 2-4.5 mm, all minimal RL are less than -10 dB. For 40G-PC composite, the minimum RL is -44.3 dB at 6.8 GHz when the material thickness is 3.5 mm, and the bandwidth less than 10 dB can reach up to 4.6 GHz (from 10.2 to 14.8 GHz).

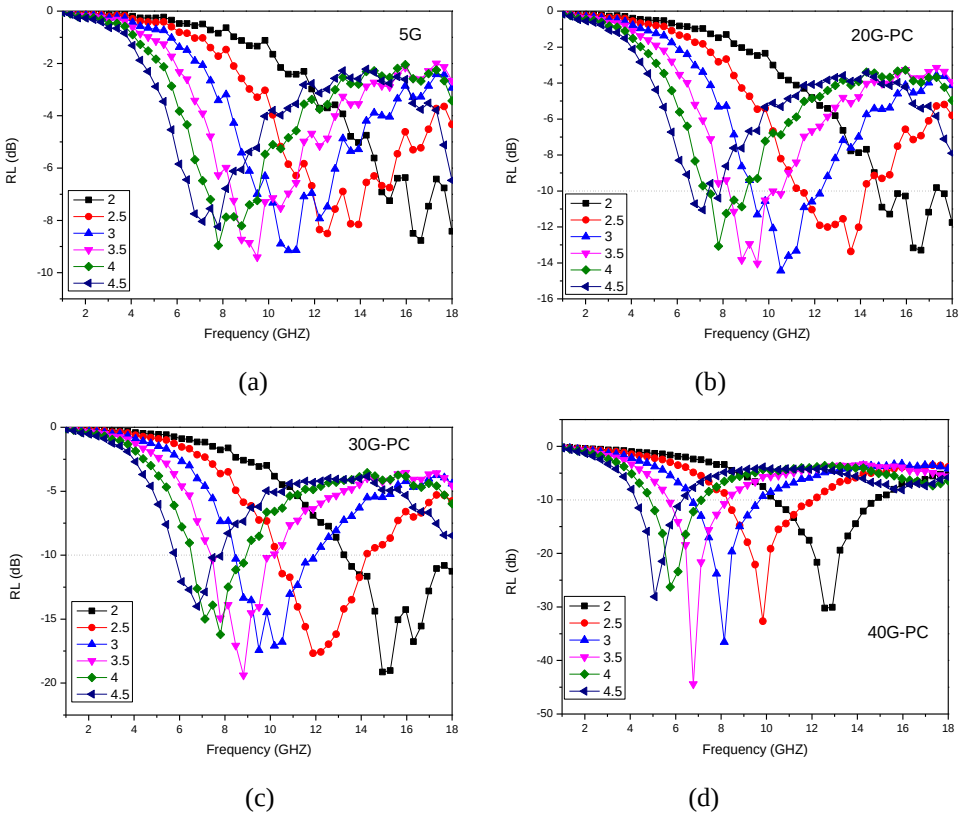

Fig. 5. Reflection loss curves of (a) G and G-PC (b-d) composites with different thickness.

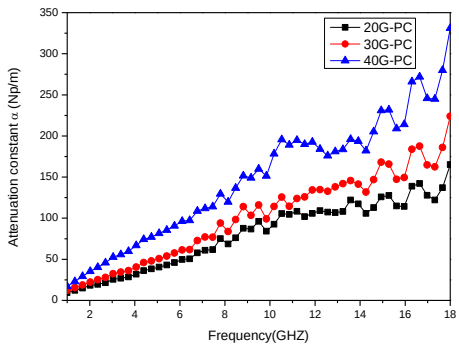

Fig. 6. Attenuation constant α of the composites.

The microwave in propagating medium should be completely absorbed through the magnetic loss and the dielectric loss. This absorption property is mainly reflected by the attenuation constant α and it can be expressed as:

$$\alpha = \frac{\pi f}{c}\left(2\left(\mu''\varepsilon'' - \mu'\varepsilon' + \left(\left(\mu''^2 + \mu'^2\right)\left(\varepsilon''^2 + \varepsilon'^2\right)\right)^{1/2}\right)\right)^{1/2} \quad (3)$$

The attenuation characteristics of the absorber can be determined by the attenuation constant. Fig. 6 shows the relationship between the attenuation constant and the frequency. The 40G-PC α value is the largest among the three composites, and as a result it displayed better microwave absorption properties. Moreover, the density of graphene–PANI@ porous CIP/epoxy composites is in the range of 0.72–0.93 g/cm^3; this shows that this kind of hybrid composite has advantages over the traditional inorganic absorbing materials in lightweight field.

4. Conclusions

In conclusion, a new type of lightweight microwave absorber was prepared by using a combination of PANI@ porous CIP and graphene sheets within an epoxy matrix. PANI was introduced to adjust the impedance, whereas porous CIP was used to enhance the interaction between the electromagnetic waves and the absorber by inducing multiple reflections.

The absorption bandwidth, with less than -10 dB RL, can reach up to 4.6 GHz with a material thickness of 2 mm for the composites with 40 wt.% of PANI@ porous CIP and 5 wt.% of Graphene. The results show that graphene-PANI@ porous CIP is a promising wave absorbing composite material.

Acknowledgments

This work was financially supported by the National Nature Science Foundation of China (No.61376064).

References

[1] W. Zhang, D. Zhang, Journal of Magnetism & Magnetic Materials **396**, 169 (2015).
[2] F. Qin, C. Brosseau, Journal of Applied Physics **111**, 6 (2012).
[3] S. Xuan, Y.J. Wang, K.C. Leung,K.Shu, Journal of Physical Chemistry C **112**,18804 (2008).
[4] P. Xu, X. Han, J. Jiang, X. Wang, X. Li, A. Wen, Journal of Physical Chemistry C **111**,12603 (2007).
[5] N.M. Barkoula, B. Alcock, N.O. Cabrera, T. Peijs, Polymers & Polymer Composites **16**,101(2008).
[6] B. Zhang, J. Wang, J.P. Wang, S.Q. Huo, Y. Tang, Journal of Magnetism & Magnetic Materials **413**,81(2016).
[7] S.B. Wen, G.W. Li, Q.Y. Wu, Advanced Materials Research **557**, 259 (2012).
[8] J. Tang, L. Ma, N. Tian, Materials Science & Engineering B **186**, 26 (2014).
[9] M.A. Abshinova, N.E. Kazantseva, P. Sáha, I. Sapurina, J. Kovářová, J. Stejskal, Polymer Degradation & Stability **93**,1826 (2008).
[10] G.X. Tong, W.H. Wu, Q. Hu, J.H. Yuan, R. Qiao, H.S. Qian, Materials Chemistry & Physics **132**,563 (2012).
[11] J. Wei, R. Zhao, X. Liu, Journal of Magnetism & Magnetic Materials **324**, 3323 (2012).

[12] J. Wang, J. P. Wang, B. Zhang, Y. Sun, W. Chen, T. Wang, Journal of Magnetism & Magnetic Materials **401**, 209 (2016).
[13] P. Liu, Y. Huang, J. Yan, Y. Zhao, Journal of Materials Chemistry C **4**,6362 (2016).
[14] S. Ni, X. Wang, G. Zhou, F. Yang, J. Wang, Materials Letters **63**, 2701 (2009).
[15] B.J.P. Adohi, V. Laur, B. Haidar, C. Brosseau, Applied Physics Letters **104**, 4184 (2014).
[16] X.F. Zhang, X.L. Dong, H. Huang, Y.Y. Liu, W.N. Wang, Applied Physics Letters **89**,1 (2006).
[17] J. Wang, R.F. Place, V. Portnoy, V. Huang, M.R. Kang, Journal of Biological Methods **2**,21 (2015).
[18] A. Aharoni, Physica Status Solidi **231**,547 (2015).